# Resonant magneto-optical properties of Fe near its $2p$ levels: Measurement and applications

J. B. Kortright and Sang-Koog Kim*
*Materials Sciences Division, Lawrence Berkeley National Laboratory, Berkeley, California 94720*
(Received 25 May 2000)

Resonant magneto-optical properties of Fe are considered across its $2p$ core levels. General equivalence of the classical magneto-optical formalism (dielectric tensor) and the resonant atomic scattering factor in the electric dipole approximation is shown in describing pure charge contributions as well as first- and second-order magnetic contributions. Thickness effects in transmission absorption measurements are considered and shown to be minimized in Faraday magneto-optical rotation measurements. Transmission absorption and Faraday rotation spectra obtained using linear polarization are normalized to the complex refractive index and atomic scattering factor for pure circular modes and their polarization average, showing that the pure magnetic part is roughly 50% of the pure charge part at the $L_3$ resonance. Magnetic linear dichroism (Voigt effect) measured in transmission is only 2% of the pure charge scattering at resonance. These magneto-optical constants are used to calculate important polarization-dependent experimental quantities including penetration depths, critical angles for total external reflection, Kerr rotation and intensity spectra, and interference and distorted-wave effects that modulate scattering intensities. The results reveal the importance of knowledge of these properties and use of full magneto-optical formalisms in planning and interpreting experiments involving resonant $2p$ optical properties of the $3d$ transition metals.

## I. INTRODUCTION

Following the prediction that optical transitions from spin-orbit split core levels to spin-polarized final states should result in large resonant magneto-optical effects,[1] a decade or more passed before naturally polarized synchrotron radiation began to be exploited at VUV and x-ray wavelengths in measurements of magnetic linear[2,3] and circular[4,5,6] dichroism and resonant magnetic scattering.[7] Resonant x-ray magneto-optical (MO) effects continue to grow in interest. This is because of their ability to provide fundamental information regarding electronic structure, including spin and orbital magnetic moments in a host of materials, and because of the increasingly apparent prospects of applying them to resolve the response of heterogeneous magnetic materials into that of individual constituent elements.[8] Such techniques enable, for example, studies of how interactions between different magnetic (and nonmagnetic) phases affect the individual phases and also the aggregate properties of the material, with the spatial resolution set by the wavelength. Resonant MO effects are strongest in the hard and soft x-ray range near dipole-allowed transitions coupling sharp core levels to spin-polarized final states and manifest themselves in a variety of ways.

Here we focus on the $2p$ levels of $3d$ transition elements in the 500–1000 eV range because they yield the largest resonant MO effects for these important magnetic elements. The first MO measurements in this range were predominantly magnetic circular dichroism (MCD) measurements using electron yield techniques,[5,6,9] which are powerful in conjunction with sum rules to resolve spin and orbital moments, but limited by their near-surface sensitivity in the scope of problems they can study. Photon-based techniques also exhibit resonant MO effects in specular reflection,[10–13] transmission,[14–18] and scattering,[19–21,17] and are of increasing interest because of their ability to penetrate more deeply than electrons and compatibility with strong and varying applied fields to study dynamics. As these techniques develop, it is important to consider more fully the range of resonant MO effects and precisely what it is that they measure. For example, following early soft x-ray MCD measurements, circular polarization and intensity measurements in photon-based reflection and scattering experiments are common, while magneto-optical rotation measurements using linear polarization common in near-visible spectral regions are also possible in the soft x-ray range. It is important to understand how the MO signals in these different measurements relate to sample magnetization and its changes. Also important are measuring and understanding the fundamental magneto-optical properties of samples in the vicinity of strong absorption lines at core levels and how these properties influence penetration depth, interference behavior in thin-film samples, and other measurable quantities. While formalisms exist to consider these questions, they have not been routinely applied to soft x-ray magneto-optical measurements. The magneto-optical properties of Fe in the region of its $2p$ levels are more fully considered here, and standard formalisms applied to consider how the fundamental properties influence different measurements of current interest. The results generalize to some extent to resonant MO properties of other $3d$ transition elements that exhibit similarly strong $2p$ absorption features.

This paper is organized as follows. Section II reviews and relates two different theoretical formalisms that can describe the MO properties of interest. Section III discusses some difficulties in the measurement of the fundamental MO constants near strong white lines and presents results for Fe. Section IV uses these measured optical constants in calculations to simulate a variety of magneto-optical properties of interest in recent and current measurements. These results show that careful attention to the details of strong resonant

 

MO effects is important in planning and interpreting soft x-ray resonant MO experiments because of the rich variety of MO effects that manifest themselves in many different ways.

## II. THEORETICAL DESCRIPTION

Magneto-optical effects are changes in polarization and/or intensity of transmitted (Faraday effects) or reflected (Kerr effects) beams on reversal or change of magnetization **M** in the sample. At least two formalisms are available to describe resonant soft x-ray MO properties. One uses the classical dielectric tensor.[22,23] Another uses the resonant atomic scattering factor including charge and magnetic contributions.[24,25] The equivalence of these two descriptions (within the dipole approximation) is demonstrated below, and some useful strengths of each approach are discussed.

The dielectric tensor $\varepsilon(\omega)$ is typically used at near visible and longer wavelengths to give the classical, macroscopic response of the medium[22] and can also describe resonant magneto-optical effects in the x-ray range.[23] In general, the rank and symmetry of $\varepsilon$ is determined by the symmetry of the single-crystal sample. The polycrystalline Fe films studied here have (110) texture with random in-plane orientation leading to significant averaging of crystallographic axes in the film plane, which contains the magnetization **M**. Thus we take the isotropic form of $\varepsilon$ (with **M** along $z$) to describe these samples:

$$\varepsilon(\omega)=\begin{pmatrix} \varepsilon_{xx} & \varepsilon_{xy} & 0 \\ -\varepsilon_{xy} & \varepsilon_{xx} & 0 \\ 0 & 0 & \varepsilon_{zz} \end{pmatrix}.$$

This description is appropriate for homogeneous, macroscopic (i.e., bulk) MO properties, but neglects effects that may result from the reduced symmetry imposed, e.g., by the interfaces of films only nanometers thick. These effects could include the very general concept of Néel's surface anisotropy[26] in which simply the broken symmetry is expected to modify the magnetic properties. Alternatively, increasingly common observations,[27–29] and theory[30] suggest that changes in local interatomic structure and bonding can influence magnetic and hence magneto-optical properties at interfaces and of ultrathin films. Even in somewhat thicker films, noncubic distortions can significantly modify structural and magnetic anisotropy and hence the effective symmetry of the dielectric tensor. Thus caution is needed in assuming that bulk homogeneous descriptions adequately describe real systems. Nonetheless, this description provides a starting point in the discussion of MO properties.

A complete description of MO effects in this formalism is given by the four nonzero elements of the dielectric tensor or, equivalently, by the complex refractive index $n(\omega)\equiv\sqrt{\varepsilon(\omega)}=1-\delta(\omega)+i\beta(\omega)$ for several normal modes corresponding to the propagation of pure polarization states along specific directions in the sample. Radiation with other polarization or incident along different directions generally experiences polarization changes on propagation. The solution of Maxwell's equations yields these normal modes,[22] one of which is for circular components of opposite $(+/-)$ helicity with wave vector $\mathbf{k}\|\mathbf{M}$ having indices $n_{+/-}=1-\delta_{+/-}+i\beta_{+/-}=\sqrt{\varepsilon_{xx}\pm i\varepsilon_{xy}}$. The two other cases are for linear polarization with $\mathbf{k}\perp\mathbf{M}$. One has electric vector $\mathbf{E}\|\mathbf{M}$ and index $n_{\|}=1-\delta_{\|}+i\beta_{\|}=\sqrt{\varepsilon_{zz}}$. The other has $\mathbf{E}\perp\mathbf{M}$ and $n_{\perp}=1-\delta_{\perp}+i\beta_{\perp}=\sqrt{(\varepsilon_{xx}^2+\varepsilon_{xy}^2)/\varepsilon_{xx}}$. The complex Faraday response $\phi_F=(n_+-n_-)\pi t/\lambda=\alpha_F-i\varepsilon_F$ contains both the induced ellipticity angle $\varepsilon_F$ and the rotation angle $\alpha_F$ describing polarization changes to the incident linear polarization (a coherent superposition of + and − helicity circular components) on propagation through the film of thickness $t$. Magnetic circular dichroism and birefringence are first order in **M** (or $\varepsilon_{xy}$) and are given by $\beta_+-\beta_-$ and $\delta_+-\delta_-$, respectively, the later representing the magneto-optical rotation (MOR) of the plane of polarization. Magnetic linear dichroism (MLD) and birefringence $n_{\perp}-n_{\|}$ (also known as the Voigt effect) are quadratic in **M**. The Voigt effect is present in both ferromagnets and antiferromagnets, while the first-order MO effects in the forward scattered beam are absent with the net magnetization in antiferromagnets, except possibly at interfaces and other defects at which spins are not compensated.

The atomic scattering factor $f(\omega,q)=f^0(q)+f'(\omega,q)+if''(\omega,q)$ provides a microscopic description of the interaction of x-ray photons with magnetic ions. Here we consider only nonresonant pure charge scattering and resonant charge and magnetic terms, all of which are much larger than nonresonant magnetic terms.[24,25] For the small values of the scattering vector $q=|\mathbf{q}|=4\pi\sin\theta/\lambda$ available near the Fe $2p$ levels, the nonresonant charge term $f^0(q)\cong Z$, where $Z$ is the number of electrons per Fe atom. Considering only electric dipole transitions yields three resonant terms with distinct dependences on incident and scattered photon polarization ($\mathbf{e}_0$ and $\mathbf{e}_f$, respectively). Together with the nonresonant charge term, the scattering factor becomes

$$\begin{aligned} f=&(\mathbf{e}_f^*\cdot\mathbf{e}_\theta)\left\{\frac{3}{8\pi}\lambda[F_1^1+F_{-1}^1]-r_eZ\right\} \\ &+\frac{3}{8\pi}\lambda\{i(\mathbf{e}_f^*\times\mathbf{e}_0)\cdot\mathbf{m}[F_{-1}^1-F_1^1]+(\mathbf{e}_f^*\cdot\mathbf{m})(\mathbf{e}_0\cdot\mathbf{m}) \\ &\times[2F_0^1-F_1^1-F_{-1}^1]\}. \end{aligned}$$

Here $r_e$ is the electron radius and **m** is a unit vector along the magnetization of the ion. The polarization dependence of the resonant terms results from the interaction of incident x-ray polarization with the vector spherical harmonics describing the transitions from $p$ to $d$ states. The different $F_M^L$ terms are dipole matrix elements from initial to final states resolved into different spherical harmonics and thus represent the spectral dependence of transitions into empty $d$ final states of specific symmetry, specific linear combinations of which are associated with distinct polarization dependences. Terms with $\mathbf{e}_f^*\cdot\mathbf{e}_0$ polarization dependence are the nonresonant and resonant charge scattering. Terms involving $(\mathbf{e}_f^*\times\mathbf{e}_0)\cdot\mathbf{m}$ are first order in **M** and yield MCD and MOR. Terms involving $(\mathbf{e}_f^*\cdot\mathbf{m})(\mathbf{e}_0\cdot\mathbf{m})$ are second order in **M** and yield MLD. While the expression above was developed explicitly for localized atomic or ionic final states, these basic terms are also found in theoretical descriptions of atomic scattering factors in itinerant metallic systems.[31]

The general equivalence of these two formalisms is seen by noting the one-to-one correspondence of terms describing the same polarization dependence for the same normal modes and is aided by comparing the refractive indices for these modes. Refractive indices are obtained from the scattering factors from $1-n(\omega)=\Sigma_i N_i r_e \lambda^2 f_i(\omega,q=0)/2\pi$, where the atomic scattering factor is evaluated for forward scattering,[32] $N_i$ is the atom number density of species $i$, $\lambda$ is the wavelength, and the sum allows for different atomic species, only some of which need the magnetic. For circular polarization propagating along **M**, the charge and first-order terms contribute to scattering, yielding the indices $n_{+/-}=1+Nr_e\lambda^2(4\pi r_e Z-3\lambda F^1_{-1/1})/8\pi^2$. Only terms first order in **M** change sign with helicity, yielding $n_+-n_-=3Nr_e\lambda^3[F^1_1-F^1_{-1}]/8\pi^2$ as the absolute helicity difference in first-order MO effects. For the two linear polarization cases in the Voigt geometry, the charge terms contribute to each case and the second-order term contributes only to the case when $\mathbf{E}\|\mathbf{M}$, yielding $n_\|=1-Nr_e\lambda^2(4\pi r_e Z+3F^1_0\lambda)/8\pi^2$ and $n_\perp=1-Nr_e\lambda^2(8\pi r_e Z+3[F^1_1+F^1_{-1}]\lambda)/16\pi^2$ with the Voigt effect $n_\perp-n_\|=3Nr_e\lambda^3[2F^1_0-F^1_1-F^1_{-1}]/16\pi^2$. Distinct expressions for the indices exist in both formalisms for the specific normal modes that propagate as pure polarization states. The three dielectric tensor elements are thus related to the three $F^L_M$ matrix elements that contain spin-resolved electronic structure information. Both formalisms also describe MO interactions of nonnormal modes having arbitrary incident polarization incident at arbitrary directions with respect to **M**. The general equivalence of the dielectric tensor and scattering factor descriptions holds only in the case considering dipole transitions contributing to *f*. Higher-order multipole terms have different polarization dependence.[24] Such higher-order magnetic terms have been observed in the hard x-ray range[33] and typically are assumed to be more common as $\lambda$ decreases, although their presence near the $2p$ levels of Fe and other $3d$ transition elements cannot be ruled out.

These expressions reveal how the spin-dependent filling of *d* states leads directly to different magneto-optical effects. First-order effects result from a net uniaxial asymmetry of spin (and orbital) states along **M** and so are probed by measurements in which the wave vector **k** has a large component along **M**. Second-order effects result from a biaxial asymmetry of the charge distribution associated with **M** (and any applied field). The Zeeman effect in atoms and molecules is an example of second-order effects, in which an applied field **H** lifts degeneracy of valence states, yielding different absorption spectra with $\mathbf{E}\|\mathbf{H}$ and $\mathbf{E}\perp\mathbf{H}$. In magnetic solids $\mathbf{B}=\mathbf{M}+\mu_0\mathbf{H}$ acts on electronic states in competition with crystal field (and other) effects which generally reduce the size of MLD, especially in cubic systems by quenching orbital moments. Nonetheless, large Fe $2p$ MLD has been observed in antiferromagnetic oxides $Fe_2O_3$ (Ref. 34) and $LaFeO_3$.[35] Only one report of resonant $2p$ MLD for metallic Fe is apparent in the literature, revealing a much smaller effect than in oxides.[36]

Each MO description is useful in considering soft x-ray experiments measuring resonant MO effects. The absorptive and sometimes the refractive parts of *n* are directly and separably measured. Since $\delta(\omega)$ and $\beta(\omega)$ are related by the Kramers-Kronig transformation (KKT), measurement of only one yields the complex index.[14] Soft x-ray scattering and reflection experiments measure signals containing both absorptive and refractive contributions, in which case knowledge of these terms separately is essential for quantitative analysis of these results. The dielectric tensor and associated formalisms developed for near-visible MO analysis[22,37] are useful for calculating intensity and polarization changes on specular reflection and transmission in magnetic structures with arbitrary incident polarization and angle, and variable magnetization with depth. The long wavelengths near the Fe $2p$ resonances limit $q$ to less than roughly 1 $Å^{-1}$, precluding measurement of scattering from nearest-neighbor interatomic interference. Scattering from features having 1 nm characteristic dimension is still possible, however. The scattering factor description is readily extended to describe both specular and diffuse scattering measurements. Atomic scattering factors can explicitly account for changes in resonant MO properties that might accompany structural and chemical gradients at interfaces and in other inhomogeneous systems, including changes in the local chemical environment that change the *d*-state hybridization and filling and hence the resonant terms in the scattering factor.[38,39]

In all descriptions both pure charge and pure magnetic contributions can be distinguished. Generally, the amplitudes for pure charge and magnetic contributions are summed in both first- and second-order MO effects considered above, foretelling interest in separating these contributions in measured intensities. The quantity $\mathbf{n}_+-\mathbf{n}_-$ describes the only pure magnetic contribution first order in **M**, and Faraday rotation is the most direct measure of this quantity, as seen below. Measuring signals containing both charge and magnetic scattering contributions through a hysteresis loop can aid in distinguishing between charge and magnetic contributions to scattering. Below it is seen that the large size of resonant optical effects provides a natural means to suppress charge relative to magnetic scattering.

## III. MEASUREMENT OF MO PROPERTIES

Very strong absorption at the $L_{2,3}$ lines makes determination of both real and imaginary components of the $2p$ resonant MO properties nontrivial, especially if one is interested in obtaining values representative of the bulk. While numerous MCD experiments have been performed and results analyzed with sum rules for spin and orbital moments, most have used secondary or total electron yield (TEY) as a measure of absorption. This technique is inherently near surface sensitive, with electron escape depths of the order of 2–4 nm in metals and typically suffers from saturation effects resulting from the interplay between short electron escape depths and the rapidly varying photon penetration depth near the $L_{2,3}$ lines.[40,41] Relatively few determinations of $3d$ transition metal MO constants have been made using photons only,[14,15,16,42] in part because of the difficulty in obtaining reliable signals that separately measure either the refractive or absorptive MO response using photons. Of these, even fewer have measured Fe layers thicker than several nm.

### A. Experimental details

Samples studied here were grown by magnetron sputtering onto smooth, low-stress, 160-nm-thick $SiN_x$ membranes

for transmission measurements with Fe layers ranging from 20 to 60 nm in thickness and were capped with 2–4 nm of amorphous SiC (Ref. 43) to prevent oxidation. Ancillary transmission x-ray microscopy measurements show no evidence of significant thickness variation or pinholes in samples grown on these membranes. Numerous measurements of MO properties were made at four different beam lines at the Advanced Light Source (bending magnet beam lines 6.3.2 and 9.3.2, and undulator beam lines 7.0 and 8.0) over the coarse of several years, and what are believed to be the most accurate results (except as noted) are presented here. Each beam line is equipped with a high-resolution grating monochromator. While most recent x-ray MO measurements typically have used elliptical polarization as close as possible to circular, linear polarization was used to measure all MO properties reported here, since it contains a coherent superposition of equal amounts of opposite-helicity circular components. Linear polarization was obtained at bending magnet beam lines by selecting radiation on the orbit plane with slits upstream of the monochromator and measured to have degree of linear polarization $P_L \cong 0.95$ (except as noted). At planar undulator beam lines radiation from the central cone was measured to have $P_L \geqslant 0.98$. In all measurements **M** was saturated along known directions using permanent magnets or varied with an applied field having a known direction.

### B. Thickness effects in transmission absorption measurements

Thickness effects can distort transmitted intensities near strong $L_3$ and $L_2$ white lines, thereby precluding accurate absorption determination. Figure 1 illustrates thickness effects in the Fe transmission spectrum for films with $t=20$, 44, and 60 nm and grazing incidence angle and $\theta=45°$ measured using off-orbit elliptical polarization having $P_C=0.6$. Each film has **M** oriented such that the $L_3$ line is enhanced relative to the $L_2$ line by MCD. Thickness effects of increasing severity with $t$ are present in all spectra in Fig. 1. Calculation of the absorption coefficient $\mu$ using $T=I/I_0=e^{-\mu t}$ yields the apparent values in Fig. 1(b), normalized from 0 to 1 in the pre- and post-edge regions to isolate the absorption just from the $2p$ resonances. Absorption values at both $L_2$ and $L_3$ lines clearly exhibit increasing systematic errors as $t$ increases.

Such thickness effects are known to complicate transmission x-ray absorption measurements, especially near strong white lines,[44,45,46] precisely where resonant MCD effects are largest. For the results in Fig. 1, possible problems of the detector linear dynamic range are overshadowed by problems imposed by the effects of spectral impurities in the incident beam as confirmed by the saturation of $I/I_0$ well above zero. Harmonics from the grating are one possible source of spectral contamination. Another is diffuse scattering from the grating, whose energy distribution is broad compared to the sharply peaked harmonics. Pinholes in samples exacerbate thickness effects and are not observed in films studied here as mentioned above. Efforts to correct measured data by assuming some amount of second-order contamination with known, smooth absorption across the Fe $2p$ region yield significant improvement in the shapes of the white lines, but small discrepancies with $t$ remain. Inserting

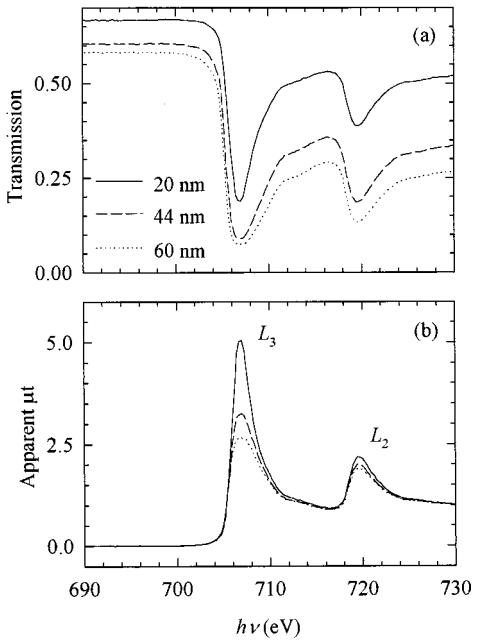


FIG. 1. (a) shows measured transmission $I/I_0$ through three Fe films having different thickness deposited onto $SiN_x$ membranes made on a bending magnet beam line with no absorption filters to surpress harmonic content in the beam. In (b) are apparent absorption coefficients obtained from $\mu t=-\ln(I/I_0)$ and the data in (a). Severe thickness effects are apparent at the $L_3$ and $L_2$ white lines (707 and 720 eV, respectively), resulting primarily from spectral contamination of the incident beam.

spectral edge filters to suppress harmonics likewise yields significant improvement, but again small discrepancies remain between samples. Spectral impurities are thus not simply the result of harmonics well separated from the fundamental, but contain energies closer to the fundamental that are not removed by absorption filters. Measurements at different beam lines and using different gratings on the same beam line are consistent with spectral contamination linked strongly to the specific grating used and signal that in practice thickness effects must always be suspected in transmission absorption measurement at white lines. Absorption from thinner samples is distorted less by thickness effects. Thus quantifying the MCD spectrum in transmission at $3d$ transmission metal $2p$ edges for all but the thinnest samples is difficult, as recognized in Ref. 15.

Utilizing a multilayer interference structure acting simultaneously as a linear polarizer and a bandpass filter[13] in the transmitted beam helps avoid thickness effects in several ways. One is by enabling measurement of Faraday rotation rather than transmitted intensity. This is demonstrated in Fig. 2, which shows Faraday hysteresis loops measured using linear polarization through the same 20-, 44-, and 60-nm Fe films at $\theta=45°$. The linear polarizer was aligned and calibrated by rotating it azimuthally to obtain a symmetric sinusoidal curve and then set at 45° azimuth with respect to the incident linear polarization to record intensity changes resulting from MOR as a longitudinal field is varied. Loops normalized to rotation angle are in Fig. 2(a) and, to specific rotation (rotation/thickness), are in Fig. 2(b). No thickness effects are evident in these data in part because this measurement was made several eV below the $L_3$ line where the

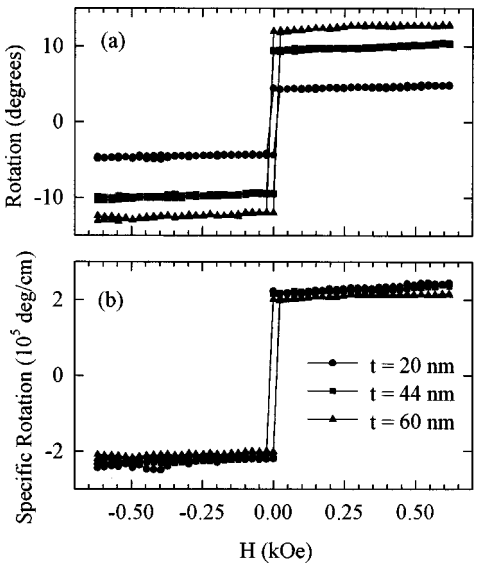


FIG. 2. Hysteresis loops measured by Faraday rotation through Fe films of three thickness as noted with $h\nu \sim 2.5$ eV below the Fe $L_3$ line. (a) shows data normalized to the absolute rotation, while (b) shows data normalized to specific rotation.

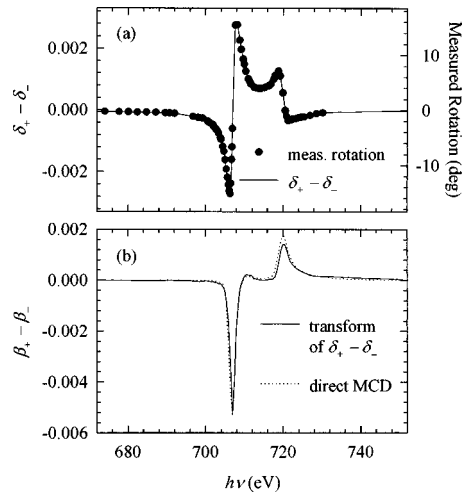


FIG. 3. Faraday rotation spectra measured through a 32-nm Fe film at 30° grazing incidence is shown in (a). Absolute rotation scale is at left, and at right are data normalized to $\delta_+ - \delta_-$. Solid circles are measured data points, and the line is a smooth fit to these data. The MCD spectrum $\delta_+ - \delta_-$ obtained from the Kramers-Kronig transformation of these data is the solid line in (b). Also in (b) is an MCD spectrum $\beta_+ - \beta_-$ measured directly in transmission through a 6–7-nm Fe film from Ref. 15. The two spectra are normalized at the $L_3$ peak.

thickness effects in absorption are less severe. Since the $\alpha_F$ spectrum passes through zero at the $L_3$ line peak (see below), it is generally desensitized to thickness effects compared to transmission absorption measurements. Moreover, the multilayer polarizer acts as a dispersive bandpass filter with bandwidth $\Delta\lambda/\lambda \cong 0.01-0.02$ and is thus a more effective wavelength filter than absorption edge filters for removing both harmonics and broadband scattered light. This further desensitizes $\alpha_F$ measurements to scattered light and also can be used in transmitted intensity measurements as perhaps the most effective way to minimize thickness effects at strong white lines in the soft x-ray range.

These considerations of thickness effects influenced our approach to determining resonant MO properties for Fe films to minimize the number of direct measures of transmitted intensity that is most prone to suffer from thickness effects, in favor of measuring the $\alpha_F$ spectrum that is less prone to thickness effects. The one required direct transmission measurement is made at normal incidence, thereby minimizing sensitivity to thickness effects for a given $t$ and avoiding the most difficult case when MCD maximizes the absorption of the stronger $L_3$ peak as in Fig. 1. The relative absence of thickness effects in the measured data below is gauged by the height of the $L_3$ line compared to the jump in the continuum absorption.

### C. Determination of first-order MO properties

This approach uses linear polarization to obtain $n_+ - n_-$ from the complex Faraday rotation spectrum $\phi_F$ containing the ellipticity angle $\varepsilon_F$ as well as the rotation angle $\alpha_F$. While $\varepsilon_F$ and hence MCD can be determined directly from polarimetry data,[16] doing so accurately requires careful measurement of absolute intensities, rather than the more easily measured phase shifts (intensity differences) needed for a rotation determination of $\delta_+ - \delta_-$. Alternatively, $\beta_+ - \beta_-$ can be obtained from KKT of $\delta_+ - \delta_-$. Comparison of both approaches reveals that the second approach more reliably determines the $\beta_+ - \beta_-$ spectrum for these data. Transmission absorption measures $(\beta_+ + \beta_-)/2$ from which $(\delta_+ + \delta_-)/2$ is obtained via KKT, yielding the polarization averaged index $(n_+ + n_-)/2$ describing the pure charge scattering.

The real part of the Faraday rotation spectrum through a 32-nm-thick Fe film at $\theta = 30°$ is in Fig. 3(a). The direction of **M** maximizes $\mathbf{k}\cdot\mathbf{M}$ at this $\theta$. Rotating analyzer scans of the tunable polarizer were made with sample in and out at energies indicated by data points, yielding absolute measured rotation that peaks at $+/-15.5°$ on either side of the $L_3$ resonance. Normalizing measured rotation by the path length in the film and by $g = \cos\theta$ ($g$ is the direction cosine between **k** and **M**) to project the result along the magnetization direction yields the $\delta_+ - \delta_-$ scale in the figure. The absolute value of these rotations, as well as the specific rotation which peaks at $2.7\times10^6$ deg/cm, are roughly an order of magnitude larger than observed at wavelengths in the IR-UV ranges. Values for specific rotation for Fe in these regions are $3.5\times10^5$ deg/cm at 564 nm (Ref. 22) and $5.1\times10^5$ deg/cm at 1000 nm.[47] Such large rotations result from the selective nature of the resonant transitions at the $2p$ levels, coupling sharp, spin-orbit split initial states to the empty final $d$ states primarily responsible for magnetism. This is just as Erskine and Stern had predicted,[1] although the $2p$ core resonances are found to exhibit larger MO effects than the $3p$ levels they considered because smaller spin-orbit splitting in the initial state tends to cancel effects from the $3p_{1/2}$ and $3p_{3/2}$ edges. Even smaller initial-state spin-orbit splitting exists in the UV-IR region, where also a broader range of initial and final states contributes to observed MO effects.

In taking the KKT of $\delta_+ - \delta_-$ to obtain $\beta_+ - \beta_-$,[48] MO contributions from other spectral ranges can be safely ignored since sharply resonant $2p$ MO effects are larger than,

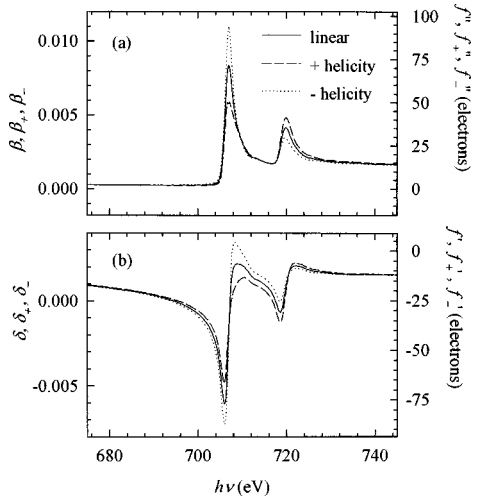


FIG. 4. First-order MO constants of Fe are plotted on two different scales corresponding to refractive index and atomic scattering factor. Linear ($\mathbf{E}\perp\mathbf{M}$) or isotropic values are also plotted. Data are accurately plotted on the $\delta$ and $\beta$ scales, but the conversion to $f'$ and $f''$ results in a slight distortion of those scales by as much as several percent at the extremes of the energy range.

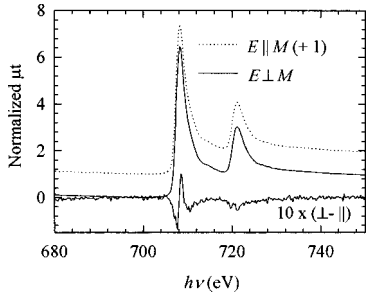


FIG. 5. Normalized transmission absorption spectra through a 32-nm Fe film at normal incidence with $\mathbf{E}\perp\mathbf{M}$ and $\mathbf{E}\|\mathbf{M}$ are offset by 1 in $\beta_\perp$ and $\beta_\|$, respectively. $\beta_\perp-\beta_\|$, multiplied by 10 and offset by 3 gives the MLD (Voigt effect).

and well separated from, resonances in other regions. The integration range in the transformation need only extend over the region where MOR is nonzero. Numerical simulation reveals that the center position of the integration range with respect to the $2p_{3/2}$ and $2p_{1/2}$ resonances is more important than the width of the range.[49]

The MCD spectrum in Fig. 3(b) results from KKT of the MOR spectrum in Fig. 3(a). The integration range was 80 eV wide and centered midway between the $2p_{3/2}$ and $2p_{1/2}$ levels. The difference of the back transformation of this MCD spectrum (same range) and the original MOR spectrum is significantly less than 1° over the entire range, with the largest discrepancy approaching 1° on the high-energy side of the $L_2$ resonance before the signal decays to zero. Superimposed in Fig. 3(b) is a transmission MCD spectrum measured through a 6-nm Fe film at $\theta=45°$ from Ref. 15. The two MCD results are scaled to the $L_3$ peak and show generally good agreement. The $L_3$:$L_2$ intensity ratio is larger for the transformed result, which by sum rule analysis would indicate a relatively larger orbital to spin moment ratio for the transformed result than for the direct MCD result. This difference between the two spectra is not a result of distortion from the KKT, since it persists as the integration range and center are widely varied. The difference could result from real differences in relative orbital to spin moments between the 32- and 6-nm-thick samples, whose microstructures are likely to be different. Alternatively, the differences could result from thickness effects in the transmission MCD result, which would manifest as a reduction in the $L_3$:$L_2$ ratio.

The polarization averaged index $n_\perp=(n_++n_-)/2$ was obtained from the transmission spectrum through the same sample oriented with $\mathbf{E}\perp\mathbf{M}$ and $\theta=90°$. The resulting $\mu t$ spectrum was scaled to tabulated absorption values[50] away from the edge where near-edge effects are insignificant, with the result plotted in Fig. 4(a) as $\beta_\perp$. The KKT of this quantity then yields $\delta_\perp$ in Fig. 4(b). In this KKT the kernel does not vanish far from the $2p$ resonances, and an integration range from 30 to 10 000 eV interpolated tabulated values for polarization-averaged absorption outside the range of measurement. Small variations in the integration range do not alter the resulting $\delta_\perp$ spectrum. Finally, $n_\pm=n_\perp\pm(n_+-n_-)/2$ yields the individual indices giving the first-order MO effects, whose real and imaginary parts are plotted along with the polarization-averaged, or pure charge, values in Fig. 4. The pure first-order magnetic scattering as measured by $\delta_+-\delta_-$ and $\beta_+-\beta_-$ is roughly 50% of $\delta_\perp$ and $\beta_\perp$, underscoring again the large size of the core resonant MO effects for $3d$ transition metals.

Comparison of first-order MO properties of Fe obtained here with published results for Fe reveals generally similar features with systematic differences. The height of the polarization-averaged $L_3$ line in Fig. 4(b) is 5.8 times the jump height from pre- to post-edge, consistent with the relative lack of thickness effects and larger than any other reported Fe $L_3$ line height obtained by either transmission,[15,40] TEY,[40,36] or scattering.[42] Possible reasons for the taller $L_3$ peak observed here include different energy resolution, thickness effects in other transmission measurements, or saturation effects in electron-yield measurements. It is also possible that different samples studied have a different average Fe $3d$ state population resulting from microstructural differences. Few data exist that directly measures the refractive MO response $\delta_+-\delta_-$,[14,42,16] from which it is apparent that Faraday rotation provides a more accurate measure than scattering.

### D. Measurement of the Voigt linear dichroism

Transmission MLD was measured at $\theta=90°$ from several samples on different beam lines by rotating the sample with saturated in-plane **M** to be parallel and perpendicular to **E** of the incident linear polarization. The individual normalized absorption spectra and resulting MLD signal for the same $t=32$ nm sample (above) are shown in Fig. 5. A Cu absorption filter and new holographic grating were used to obtain these data, whose strong $L_3$ line [stronger than in Fig. 4(b)] suggests minimal thickness effects. The maximum dichroism of 2% is sharply peaked at the $L_3$ line with broader features extending to higher energy and at the $L_2$ line. The bipolar character of the dichroism signal suggests that it may result simply from small energy shifts between scans. This can be ruled out both by repeated measurements (same day and months apart) and by numerical simulations of the difference

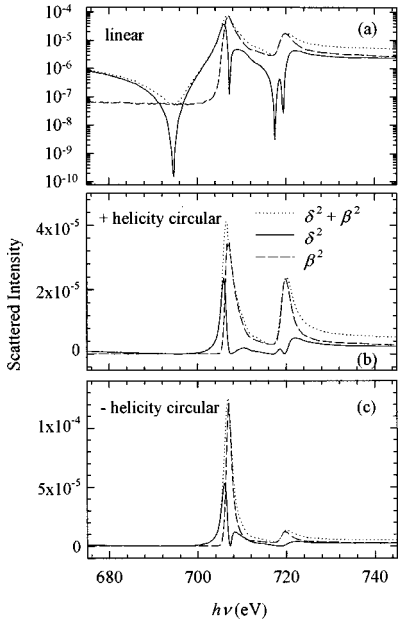


FIG. 6. Calculations of the scattered intensity based on measured MO constants are resolved into refractive ($\delta^2$) and absorptive ($\beta^2$) contributions and their sum in (a), (b), and (c) for linear (isotropic), plus-, and minus-helicity circular components, respectively. The data in (a) are plotted on a logarithmic scale to reveal weak features.

of a given measured absorption curve with itself after small energy shifts, which show that the measured MLD is not consistent with a simple energy shift. The sharply peaked structure is similar in shape to that in Ref. 36 and results rather from a small magnetization-induced redistribution of Fe $d$ states.

## IV. APPLICATIONS

While of fundamental interest since they provide, in conjunction with sum rule analysis, direct measures of the spin and orbital moments, the MO properties of Fe are also directly relevant in planning and interpreting a wide range of experimental studies involving resonant MO effects. The large size of the first-order MO effects of Fe (and other $3d$ transition elements) produce surprisingly large optical effects that can both enable and complicate experimental studies, as demonstrated below. For metallic Fe the second-order MO effects are an order of magnitude smaller than first-order effects and are ignored in this discussion.

### A. Scattered intensity spectra

The scattering amplitudes for different polarization states expressed in Fig. 4 as atomic scattering factors or as $1-n=\delta+i\beta$ (the difference from 1 representing the scattering difference from vacuum) underlie all intensity and phase effects measured in experiments. The scattered intensity spectra obtained as $(\delta+i\beta)(\delta-i\beta)$ or, equivalently, from the scattering factor exhibit large resonances at the $L_{2,3}$ levels that contain separate contributions from the real and imaginary parts of the amplitude for the different normal modes. These individual contributions and their sum are plotted Fig. 6 for the three normal modes (linear and opposite helicity circular).

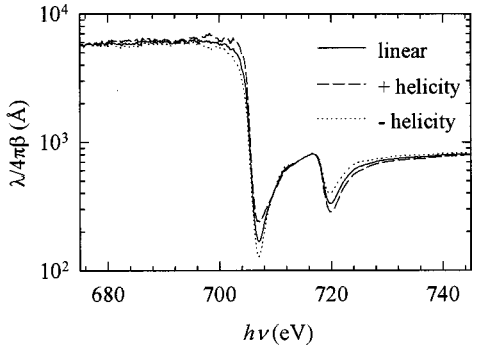


FIG. 7. The $1/e$ penetration depth $\lambda/4\pi\beta$ for normally incident radiation vs energy is strongly polarization dependent as calculated using measured MO constants. The values for + and − helicities are projected onto the direction of $M$, while the linear (isotropic) value is appropriate for unpolarized radiation or linearly polarized radiation and represents the skin depth in the absence of MO effects.

While the shapes of the total intensity are qualitatively similar to the absorption spectrum, with large peaks at the $L_3$ and $L_2$ white lines, it is important to realize that they contain both refractive and absorptive contributions. The imaginary contribution follows the absorption spectrum, while the refractive contribution is significant below the $L_3$ line, where it can be several orders of magnitude larger than the absorptive contribution. At and above the $L_3$ line, the absorptive component is dominant. Unlike $\beta^2, \delta^2$ shows several sharp spectral features, most evident in Fig. 6(a) where intensities for linear polarization are plotted on a logarithmic scale. These four sharp minima correspond to energies where $\delta$ passes through 0 (or $f'$ through $-Z$); these conditions result simply from the extremely large, sharp white lines representing the large number of empty $3d$ holes. Minima occur at each white line position, and each has a corresponding minimum below the line where the refractive amplitude passes through 0 in the other direction. The energies of these points below the white lines vary with polarization as the size of the resonance varies. Thus, at 694.7 eV, where $\delta$ vanishes for linear polarization, the real part of the charge scattering is zero, while the real part of the magnetic scattering can still have appreciable amplitude. Tuning to $\delta_{+/-}=0$ for either circular component causes the real part of the charge plus magnetic scattering to be zero for that helicity. These zero crossings have important implications for measurable optical and MO properties, some of which are seen below.

### B. Penetration depth

The penetration depth for the electric field intensity at normal incidence, $\lambda/4\pi\beta$, is polarization dependent and a strong function of $h\nu$ across the $2p$ spectrum as in Fig. 7. Below the $L_3$ edge radiation penetrates hundreds of nm into an Fe sample. Strong $L_3$ absorption significantly reduces penetration to 13 and 24 nm for the two circular components at the peak (assuming $g=1$). As grazing incidence is approached, these skin depths scale as $\sin\theta$ until near the critical angle for total reflection. Thus, at $\theta=15°$, commonly

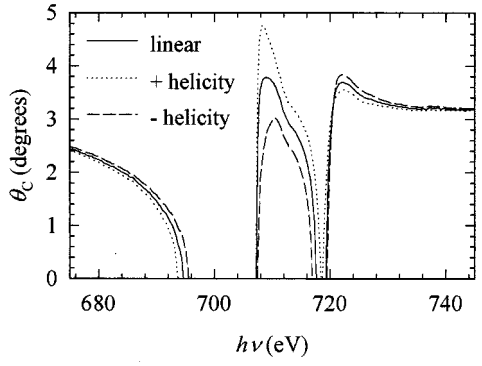


FIG. 8. The critical angle for total external reflection, $\theta_c = \sqrt{2\delta}$, is strongly energy dependent for a given polarization and shows strong differences with polarization in these calculations based on measured MO constants. When $\delta$ is negative, incident radiation refracts into the sample and exhibits total internal reflection. When $\delta = 0$ the real part of the scattering goes to zero.

used to study samples with in-plane **M**, the penetration depth is only 3 and 6 nm for the circular components. These values are comparable to typical electron escape depths, signaling the need to correct for saturation effects in total electron yield measurements of absorption, as discussed in Refs. 40 and 41. The helicity dependence of the x-ray penetration depth leads to helicity-dependent saturation effects, with the more strongly absorbed helicity suffering stronger effects. This asymmetry in saturation effects is not explicitly considered in these references and, if done so, leads to slightly larger correction factors.

In contrast to the limited penetration when the MCD signal $\beta_+ - \beta_-$ is strong, the MOR signal $\delta_+ - \delta_-$ remains large at least several eV below the $L_3$ line. Reflection geometry measurements sensitive to this signal can thus obtain strong MO sensitivity and significant penetration (100 nm at $\theta = 10°$) simultaneously. This can be important in studying the reversal process of relatively thick soft Fe layers exchange coupled at deeply buried interfaces to layers having very different anisotropy, as in recently developed exchange-spring systems.[51]

### C. Critical angle for total external reflection

Large optical effects occur at small grazing incidence angles in the region where the total external reflection is typical in the x-ray region. The critical angle for the total external reflection is given by $\theta_c = \sqrt{2\delta}$ and is plotted for $+/-$ helicity (magnetic plus charge) and linear (charge only) scattering in Fig. 8. The dispersive resonances associated with the $L_3$ and $L_2$ lines are strong enough that $\theta_c$ vanishes when $f' < -Z$ electrons and $\mathrm{Re}[n] > 1$, in which case incident radiation refracts into the sample rather than toward the sample surface. In the transition from total external to total internal reflection, the optical properties pass through the zero-refraction condition when $\delta$ passes through 0. Not only are the resonant dispersive effects quite large, but their polarization dependence is likewise large, as seen by the distinct differences in the $\theta_c$ curves for the different polarizations. Both the reflected intensity and phase change on reflection (which varies by $\pi$ from $\theta = 0$ to $\theta = \theta_c$) are now strong functions of polarization and so can produce striking MO effects in experiments operating near this angular range.

### D. Specular scattering: X-ray magneto-optic Kerr effects

Just as the Faraday (transmission) MO formalism is seen above to extend into the x-ray range, so do Kerr (reflection) MO effects and formalisms. Typically discussed in terms of longitudinal, transverse, or polar limiting cases depending on directions of **k** and **M**, MO Kerr effects produce polarization and/or intensity changes in the reflected beam as the sample magnetization changes.[22] While refractive and absorptive contributions remain separate in the complex Faraday MO response $\phi_F$, they are not separate in the complex Kerr MO response $\phi_K$, which contains terms involving products of refractive and absorptive contributions. Thus direct measurement of MO properties is facilitated by the transmission geometry, although may be possible by fitting and analyzing the spectral dependence of $\phi_K$.

General formalisms exist to calculate MO Kerr effects for radiation of arbitrary polarization and incidence angle onto structures having arbitrary distributions of **M** with depth.[37] Such formalisms typically consider only first-order MO effects, in which case $\varepsilon$ takes the form

$$\varepsilon = n_0^2 \begin{pmatrix} 1 & iQ & 0 \\ -iQ & 1 & 0 \\ 0 & 0 & 1 \end{pmatrix},$$

where $n_0 \equiv (n_+ + n_-)/2 = n_\perp$ represents the isotropic or pure charge scattering and the Voigt constant $Q \equiv i\varepsilon_{xy}/\varepsilon_{xx}$ gives the magnetization dependent part of the first-order MO response of the medium with $\mathbf{M} \| z$. The indices for circular components are now $n_\pm = n_0(1 \pm gQ)$, where $n_0$ gives the pure charge forward scattering. Formalisms using this approach are directly transferable to the x-ray range, where $n_0$ and $Q = (n_+ - n_-)/n_0$ are determined from data above. While resonant MO scattering is very large, it remains smaller than pure charge scattering, and with $n_{+,-,0} \approx 1$, $Q < 1$, so that approximations ignoring higher-order terms in $Q$ of most MO formalisms remain valid. Several calculations using the matrix method developed by Zak *et al.*,[37] which easily accounts for layered magnetic structures, are given below. This formalism uses a matrix approach to calculate the Kerr matrix of reflected amplitudes for *s* and *p* components, $\begin{pmatrix} r_{ss} & r_{sp} \\ r_{ps} & r_{pp} \end{pmatrix}$, in which off-diagonal terms yield polarization changes on reflection. The complex Kerr rotation is $\phi_{K,s} = r_{ps}/r_{ss}$ for incident *s* polarization, with a similar expression for incident *p* polarization. For each case, $\phi_K = \alpha_K + i\varepsilon_K$, where rotation and induced ellipticity are given by the real and imaginary parts, respectively. The Kerr intensity is the total field intensity reflected for an incident field having arbitrary polarization.

Longitudinal MO effects for Fe calculated using measured optical constants are shown in Fig. 9. The top panel shows the Kerr intensity for linear (*s*-component) and $+/-$ helicity circular components incident on a semi-infinite Fe sample at $\theta = 15°$. The specular scattering shows large resonant enhancements at the $L_3$ and $L_2$ lines. The resonant enhancements for $+/-$ helicity and their difference appear similar to the respective $\beta$ and MCD spectra, but are not

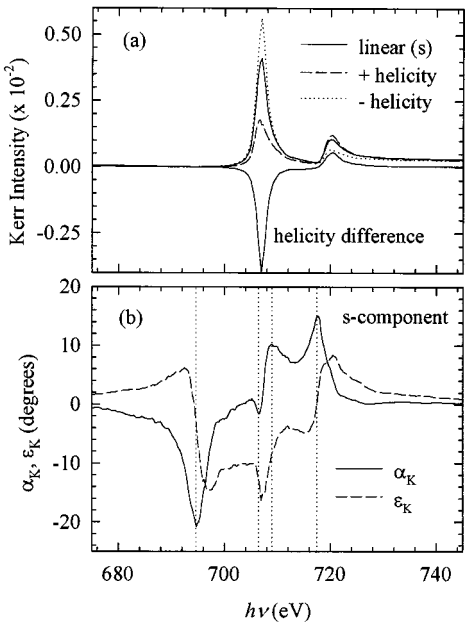


FIG. 9. Calculated longitudinal Kerr MO effects calculated for $\theta=15°$ using measured MO properties for a semi-infinite Fe sample. Kerr intensities for different polarizations as noted are in (a), and Kerr rotation and ellipticity for incident *s* polarization are in (b). Vertical lines at 694.7, 706.5, 709.0, and 717.5 eV are at local maxima in rotation as discussed in the text.

quantitative measures of these quantities. The reflected intensities contain refractive as well as absorptive contributions like the scattered intensities in Fig. 6. Kerr intensities for opposite helicity thus are not symmetric about their polarization average, as is $\beta$. This has important implications for hysteresis measurements using the Kerr intensity as discussed more below. For $\theta$ in the range of $\theta_c$, Kerr intensity spectra have very different appearance, lacking prominent peaks at the absorption lines and showing features more correlated with those in refraction spectra.

Calculated Kerr rotation and ellipticity spectra for linear (*s*-component) polarization are shown in Fig. 9(b). The rotation goes through zero at the $L_3$ peak where the specific rotation is zero, yet does not show extrema at the same resonant positions as the Faraday rotation in Fig. 3(a). Several different resonant optical effects explain the shape of the rotation spectrum. The maximum rotation at 694.7 eV coincides with the energy at which the real part of the pure charge scattering ($\delta_0$) passes through zero and, hence, the position where the purely magnetic contribution is maximum relative to charge scattering. The MOR $\delta_+ - \delta_-$ is never zero through this region, although its size relative to $\delta_0$ decreases on either side of the peak rotation, causing the rotation to decrease away from this peak. The maximum at 717.5 eV corresponds to another condition where the pure charge scattering goes to zero. The relatively small rotation values on either side of the $L_3$ peak compared to the larger values at 694.7 and 717.5 eV result from limited penetration into the sample. The local minima and maxima at 706.5 and 709.0 eV correspond closely to those observed in the Faraday rotation spectra in Fig. 3(a). Kerr ellipticity features are the KKT of the rotation features; $\varepsilon_K$ exhibits a bipolar resonance at the points where $\alpha_K$ peaks when $\delta_0=0$. The largest ellipticity is right at the $L_3$ line, as expected due to MCD. Ellipticity remains large over the entire region in which resonant MO effects are large, which can be understood to result from significantly different values for reflectance of + and − helicity circular components in this range and suggests possible application as a Kerr elliptical polarizer in this range.

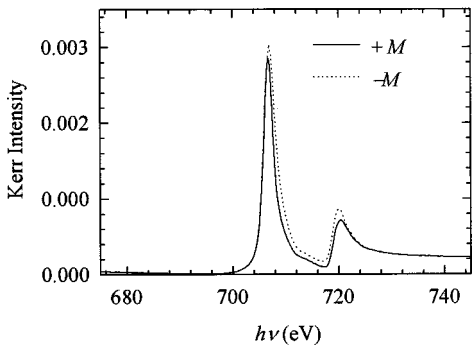


FIG. 10. Calculated transverse Kerr MO effect calculated for incident *p* polarization at $\theta=15°$ using measured MO properties for a semi-infinite Fe sample. The two curves correspond to opposite directions for transverse **M**.

In the transverse geometry the predominant Kerr MO effect is an intensity change on reversal of transverse **M** for incident linear *p* polarization. Calculations for this effect for semi-infinite Fe at $\theta=15°$ are shown in Fig. 10. Again, the difference spectrum on **M** reversal (not shown) is qualitatively similar to the MCD spectrum, but is not a quantitative measure of MCD. Linear *s* and circular incident radiation exhibit no MO effects on **M** reversal in the transverse geometry, so that Kerr intensity using incident *p* radiation is an effective means of sensing changes in net transverse magnetization. Even so, the values of reflected intensity for incident *s* and circular radiation are quite different from that for incident *p* radiation. The calculated asymmetry ratio $(I_{M+}-I_{M-})/(I_{M+}+I_{M-})$ is 6% at $\theta=15°$ and increases to 15% at $\theta=30°$, in rough agreement with measured transverse Kerr effect from a thin Fe film by Kao *et al.*[10]

The assumption of a semi-infinite sample illustrates how certain optical effects contribute to the shape of resonant Kerr MO spectra, but ignores interference effects in layered or thin-film structures that constitute a large fraction of samples of current interest. These effects become significant for an Fe layer on a substrate as its thickness decreases below roughly 0.5–1 $\mu$m in the grazing incidence regime considered here. Figure 11 illustrates these effects calculated for longitudinal Kerr intensity and rotation of incident *s* polarization for a range of thickness of Fe from 5 to 500 nm. Interference in both intensity and rotation is most prevalent below the $L_3$ edge where penetration is greatest. Interference oscillations increase in frequency with thickness and correlate in the intensity and rotation spectra. The effects are quite large and can either enhance or diminish both the Kerr intensity and rotation. Interference effects can cause the sense of the rotation to reverse. Thus care must be taken when using either the Kerr intensity or rotation as a measure of hysteresis, since apparent magnetization reversal and large changes in magnitude between samples with different layer thickness, or the same sample at different $\theta$, can result simply from interference effects. Alternatively, these interfer-

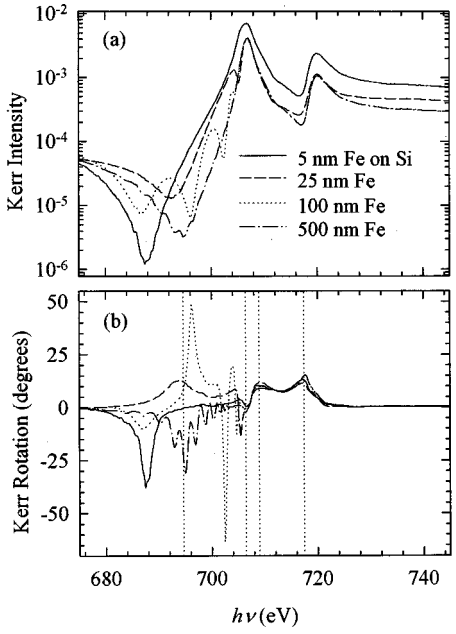


FIG. 11. Calculated interference effects in longitudinal Kerr MO effects calculated for incident *s* polarization onto an Fe film on a Si substrate with thickness as noted. The Kerr intensity is in (a) and Kerr rotation in (b). Vertical lines at the same energies as those in Fig. 9 can be used to compare how interference influences Kerr effects.

ence effects measured either as a function of energy or $q$ can be analyzed to yield information about the depth variation of magnetization in layered structures.

There is growing interest in using resonant Kerr and Faraday effects to measure the field-dependent behavior of layered structures,[12,52–54,13,17] with results in some cases analyzed semiquantitatively to infer specific details about the magnetization of different layers and their reversal. Just as optical effects can strongly influence the spectral dependence of Kerr effects, they can also influence the shape of hysteresis loops measured as **M** is varied through a hysteresis cycle. Thus it is important to consider how measured signals relate to changes in **M**.

Magnetization reversal measured using Kerr rotation of *s* polarization and Kerr intensity changes of circular polarization on longitudinal **M** reversal are simulated here. Such simulations require specific assumptions about the nature of the magnetization reversal. Here reversal is assumed to occur with no net transverse **M** component (such as would be present during a coherent rotation process) and, hence, to be representative of reversal dominated by nucleation and growth or domain wall motion. In this case the magnitude of **M**, or equivalently $Q$, reverses linearly, passing through zero in the process, ignoring coercivity mechanisms and effects. Resulting hysteresis loops of the Kerr signals vs **M** then do not resemble loops from real ferromagnetic materials, but do show features revealing the correlation between the Kerr signals and **M**. Figure 12 shows such calculated loops for the Kerr signals from semi-infinite Fe and a 10-nm Fe layer on Si at $\theta = 15°$. Each signal was calculated at seven energies as noted. Kerr rotation signals are plotted in degrees of rotation, to which measured data are easily normalized. Kerr intensity

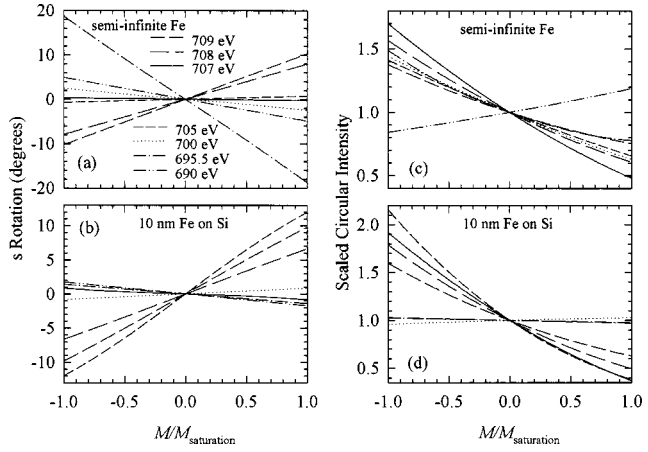


FIG. 12. The calculated effect of longitudinal magnetization reversal on different Kerr signals is shown for the cases of linear and circular polarization incident at $\theta = 15°$ onto semi-infinite Fe and [(a) and (c)] and onto a 10-nm Fe film on Si [(b) and (d)] at a variety of energies as noted. Kerr rotation of *s* polarization is in (a) and (b). Kerr intensity using circular polarization is in (c) and (d). Assumptions about magnetization reversal are in the text.

signals are normalized by their value at $\mathbf{M} = 0$ since they vary by orders of magnitude for different energies (see Figs. 6 and 9).

From calculated results in Fig. 12, it is evident that x-ray Kerr effects do not provide a unique measure of magnetization through its reversal (as they also do not in the visible). Considering first the semi-infinite Fe sample, the Kerr intensity signal is generally not linear in **M**: nor is it symmetric about $\mathbf{M} = 0$. Both of these effects are expected from the asymmetry about the pure charge scattering of the intensities of charge plus magnetic scattering for the circular components (Figs. 6 and 9). Thus care must be taken in drawing conclusions about the magnetization reversal behavior based solely on Kerr intensity data. The Kerr rotation signal is usually (although not always) linear in **M** and is always symmetric about the $\mathbf{M} = 0$ condition. This increased symmetry of rotation over intensity results because each helicity is present in the incident linear (*s*) polarization assumed in the rotation measurement. However, rotation signals are not constant in magnitude with energy and can change sign more readily with energy than intensity signals, since rotation is more sensitive to the relative phase differences of circular components than is intensity. As interference effects are included [Figs. 12(b) and 12(d)], these general trends are maintained. Interference effects generally increase Kerr intensity signals and also their asymmetry about $\mathbf{M} = 0$. Interference effects can cause rotation signals to change sign and vary widely in magnitude depending on specific conditions.

Together, these results imply that it is not generally possible to infer absolute magnetization information from resonant Kerr MO signals even from saturated samples and that inferring details about the reversal behavior from subtle differences in shapes must be done with care. The Kerr rotation should provide more accurate shapes than the Kerr intensity, although it will also show a broader variability of intensities (including sign changes). Faraday effects (in transmission) provide a much more robust quantitative measure of **M** during reversal, with the rotation less prone to artifacts than the intensity as discussed above.

### E. Diffuse off-specular scattering

The Faraday and Kerr MO effects considered above result from magnetization spatially averaged over the coherence volume of the illuminating radiation, with possible allowance for interference effects from depth-graded or layered structures. MO effects in diffuse scattering result from magnetization heterogeneity in the plane of thin-film samples within this illuminated volume. Diffuse scattering is thus an extension of the interference effects considered above, but now resulting from the interference of scattering from lateral inhomogeneity. Diffuse scattering thus necessarily reduces the intensity of the forward-scattered or specular beam. The $q$ dependence of the diffuse scattering can be related to the spatial distribution of the heterogeneous scattering object, whose Fourier transform gives the structure factor $S(q)$. The goal of diffuse scattering measurements is generally to determine $S(q)$ from this intensity distribution.

The hypothesis that magnetic and chemical surface roughness may be different has recently been investigated by diffuse scattering studies in the reflection geometry.[19,20,55,56] Some studies assume that magnetic roughness is given by the difference $(I_+ - I_-)$ and chemical roughness by the sum $(I_+ + I_-)$ of diffuse intensity measurements using circular polarization with reversed helicity or **M**. Experimental measurements of diffuse scattering in nonspecular, reflection geometry rocking scans observe that $(I_+ - I_-)$ and $(I_+ + I_-)$ both exhibit broad diffuse peaks centered at $q_x = 0$.[19,20] The width of the $(I_+ - I_-)$ scattering is narrower than that for the $(I_+ + I_-)$ scattering, leading to the conclusion that magnetic roughness has a longer in-plane correlation length or characteristic length scale than chemical roughness. Interpretation of these results is complicated by considerations of the interference between charge and magnetic contributions.[55,55] Studies to date have assumed the Born approximation, which ignores strong scattering effects such as those near the critical angle for total external reflection that lead to multiple scattering. A simple way to include these strong scattering effects is to use the distorted-wave Born approximation,[57] in which they are included in a modified incident wave field, the distorted-wave field, that then scatters from the sample.

Here it is shown that the resonant MO properties of a rough Fe surface yield very different distorted-wave fields for opposite helicity or **M** direction that significantly affect the shapes of individual sets of scattering data. The differential scattering cross section in the distorted-wave Born approximation for the off-specular scattering geometry for a semi-infinite medium is given by

$$\frac{d\sigma}{d\Omega} = \frac{(L_X L_Y)}{16\pi^2} |k_0^2(1-n^2)|^2 |T(k_1)|^2 |T(k_2)|^2 S(q),$$

where $k_0$ is the magnitude of the wave vector incident from vacuum and $k_1$ and $k_2$ are the (possibly complex) wave vector magnitudes of the incident and scattered field in the medium comprising the surface having complex index $n$ and surface roughness described by $S(q)$.[58] Here $(L_X L_Y)$ is the illuminated surface area. The factors $|T(k_{1,2})|^2$ represent the intensity of the electric field at the surface of the scattering medium and are strong functions of the index $n$ of the medium and its intrinsic optical properties (reflectivity, absorption, transmission, phase change on reflection and transmission) and their dependence on $k_1$ and $k_2$. Assuming that this expression gives the scattered intensity for circular components of opposite helicity as accounted for in $n$ and $|T(k_{1,2})|^2$, the simplest case is perfect correlation between magnetic and chemical roughness, so that both are described by the same, arbitrary $S(q)$, and that the magnetization is saturated in the film plane and in the scattering plane. In this case the scattering intensity for opposite helicity circular components is given by

$$I_\pm \propto |T_\pm(k_1)|^2 |T_\pm(k_2)|^2 S(q)$$

and the difference with helicity or **M** reversal by

$$I_+ - I_- \propto [|T_+(k_1)|^2 |T_+(k_2)|^2 - |T_-(k_1)|^2 |T_-(k_2)|^2] S(q).$$

A similar expression exists for the polarization average $I_+ + I_-$. Determination of the structural function $S(q)$ in this approach requires knowledge of the MO $|T_\pm(k_{1,2})|^2$ factors.

Calculation of the $|T_\pm(k_{1,2})|^2$ factors is straightforward using their definitions in Ref. 58, standard MO formalisms, and the optical constants for opposite helicity circular components for an Fe medium. Figure 13 contains results of calculations at a series of energies spanning the $L_3$ peak for fixed scattering angle $2\theta = 15°$ with $\theta$ varying from 0 to 15°. Results are plotted vs in-plane scattering vector $q_\parallel$ with helicity difference of $|T(k_1)|^2 |T(k_2)|^2$ in the top panel and the asymmetry ratio $(I_+ - I_-)/(I_+ + I_-)$ in the bottom panel. Both sets of curves predict a significant $q$-dependent shape of these diffuse scattering quantities for a given photon energy and strong variation of this shape with $h\nu$ based solely on the magneto-optical properties of the average surface. $|T(k_1)|^2 |T(k_2)|^2$ for each helicity and energy (not shown)

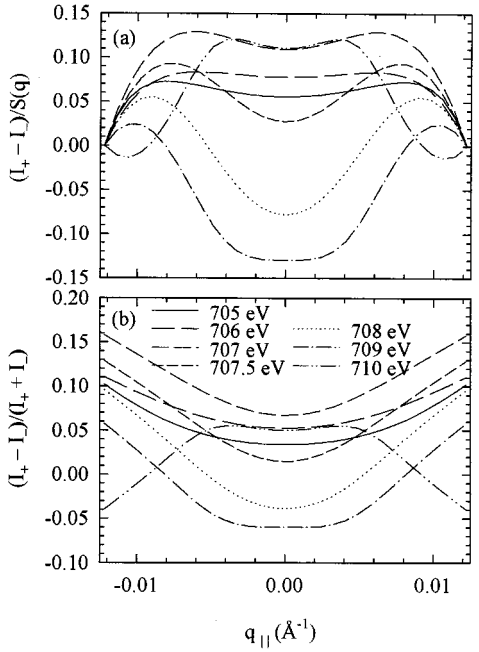


FIG. 13. Calculated optical functions (described in the text) needed in the analysis of diffuse scattering in the distorted-wave Born approximation from a semi-infinite Fe sample simulating a rocking scan at $2\theta = 15°$ for the energies noted. (a) shows the helicity difference of these optical functions, and (b) shows the helicity difference over the helicity sum.

are symmetric about $q_{\parallel}=0$, with shapes determined by the complex dependence of the Kerr intensity on angle and energy in the vicinity of strong resonances. The difference and sum of this quantity will each likewise have $h\nu$-dependent shapes symmetric about $q_{\parallel}=0$, as will the ratio of these two quantities. The range of shapes of both the polarization difference and the asymmetry ratio with energy shows that the optical effects included in the distorted-wave Born approximation are large enough to have a significant bearing on the shapes of measured curves and thus must be corrected for to obtain a reliable determination of $S(q)$. Indeed, the overall curvature of these functions can change with $h\nu$, thereby possibly reversing conclusions about the relative coherence lengths of charge and magnetic roughness. While these simulations do not specifically address the data and conclusions of the studies in Refs. 19 and 20, they suggest that the analysis should be reconsidered including distorted-wave effects as well as interference effects that are another source of modification to the distorted-wave field at the surface.

## V. SUMMARY

In the dipole approximation the resonant atomic scattering factor and the classical dielectric tensor provide equivalent descriptions of the intensity and polarization (phase) effects of specific normal modes of the forward and specular scattered beams in the Faraday and Kerr magneto-optical effects. While not surprising, this equivalence has implications that are not clearly generally appreciated. For example, in the analysis of resonant magnetic scattering experiments the change in polarization of incident and scattered beams due to their propagation through the magnetic sample does not appear to be generally taken into account. Such effects are routinely considered in generalized magneto-optical analyses.

Measurement of MO constants near strong $L_{2,3}$ white lines for the $3d$ transition elements is generally nontrivial for many reasons. With care, thickness and saturation effects can be minimized. A multilayer linear polarizer in the transmitted beam minimizes stray light in both Faraday rotation and transmitted intensity measurements. While we have considered Fe here for completeness, the general trends in resonant MO properties for Fe are also present for other $3d$ transition metals exhibiting strong white lines (V–Ni). The possible variation of MO properties near interfaces and in heterogeneous systems presents additional problems in measuring MO constants.

Standard formalisms from visible magneto-optics and scattering approaches were used to calculate a variety of MO effects based on measured MO constants. Such analyses have not generally accompanied early experimental MO studies in the soft x-ray range and are shown here to be valuable in planning and interpreting a wide range of MO experiments. In general, intensity effects using circular polarization, while easily measured, are not symmetric with regard to helicity or **M** reversal and so can lead to a misinterpretation of results if not applied with care. MO rotation signals measured using linear polarization, while somewhat harder to measure, are generally symmetric on **M** reversal and hence less prone to misinterpretation. These considerations are especially important since **M** reversal is an important means of separating magnetic from pure charge contributions to measured signals. The large size of resonant magneto-optical effects for Fe results in conditions where charge scattering is naturally suppressed relative to magnetic scattering and may provide an alternative means of separating magnetic from charge scattering in intensity measurements. Like in other spectral regions, direct measurement of polarization rotation resulting from MO effects may provide the best method of separating magnetic from charge scattering in the soft x-ray range. In general, the experimental and analytical tools exist to treat both intensity and phase effects, which together will provide maximum information regarding questions of interest.

## ACKNOWLEDGMENTS

This work and the ALS were supported by the Director, Office of Science, Office of Basic Energy Sciences, Materials Sciences Division, of the U.S. Department of Energy under Contract No. DE-AC03-76SF00098.

*Present address: Department of Physics and Center for Nanospinics of Sprintronic Materials, Korea Advanced Institute of Science and Technology, Taejon 305–701, Korea.

[1] J. L. Erskine and E. A. Stern, Phys. Rev. B **12**, 5016 (1975).
[2] B. T. Thole, G. van der Laan, and G. A. Sawatzky, Phys. Rev. Lett. **55**, 2086 (1985).
[3] Ch. Roth, F. U. Hillebrecht, H. B. Rose, and E. Kisker, Phys. Rev. Lett. **70**, 3479 (1993).
[4] G. Schütz, W. Wagner, W. Wilhelm, P. Kienle, R. Zeller, R. Frahm, and G. Materlik, Phys. Rev. Lett. **58**, 737 (1987).
[5] C. T. Chen, F. Sette, and S. Modesti, Phys. Rev. B **42**, 7262 (1990).
[6] J. G. Tobin, G. D. Waddill, and D. P. Pappas, Phys. Rev. Lett. **68**, 3642 (1992).
[7] D. Gibbs, D. R. Harshman, E. D. Isaacs, D. B. McWhan, D. Mills, and C. Vettier, Phys. Rev. Lett. **61**, 1241 (1988).
[8] J. B. Kortright, D. D. Awschalom, J. Stöhr, S. D. Bader, Y. U. Idzerda, S. S. P. Parkin, I. K. Schuller, and H.-C. Siegmann, J. Magn. Magn. Mater. **207**, 7 (1999).
[9] Y. Wu, J. Stöhr, B. D. Hermsmeier, M. G. Samant, and D. Weller, Phys. Rev. Lett. **69**, 2307 (1992).
[10] C. Kao, J. B. Hastings, E. D. Johnson, D. P. Siddons, G. C. Smith, and G. A. Prinz, Phys. Rev. Lett. **65**, 373 (1990).
[11] J. M. Tonnerre, L. Séve, D. Raoux, G. Soullié, B. Rodmacq, and P. Wolfers, Phys. Rev. Lett. **75**, 740 (1995).
[12] C. T. Chen, Y. U. Idzerda, H.-J. Lin, G. Meigs, A. Chaiken, G. A. Prinz, and G. H. Ho, Phys. Rev. B **48**, 642 (1993).
[13] J. B. Kortright, M. Rice, S.-K. Kim, C. C. Walton, and T. Warwick, J. Magn. Magn. Mater. **191**, 79 (1999).
[14] J. B. Kortright, M. Rice, and R. Carr, Phys. Rev. B **51**, 10 240 (1995).
[15] C. T. Chen, Y. U. Idzerda, H.-J. Lin, N. V. Smith, G. Meigs, E. Chaban, G. H. Ho, E. Pellegrin, and F. Sette, Phys. Rev. Lett. **75**, 152 (1995).
[16] J. B. Kortright, S.-K. Kim, T. Warwick, and N. V. Smith, Appl. Phys. Lett. **71**, 1446 (1997).

[17] J. B. Kortright, S.-K. Kim, and H. Ohldag, Phys. Rev. B **61**, 64 (2000).
[18] H.-Ch. Mertins, F. Schafers, X. Le Cann, A. Gaupp, and W. Gudat, Phys. Rev. B **61**, R874 (2000).
[19] J. F. MacKay, C. Teichert, D. E. Savage, and M. G. Lagally, Phys. Rev. Lett. **77**, 3925 (1996).
[20] J. W. Freeland, V. Chakarian, K. Bussman, Y. U. Idzerda, H. Wende, and C.-C. Kao, J. Appl. Phys. **83**, 6290 (1998).
[21] H. A. Dürr, E. Dudzik, S. S. Dhesi, J. B. Goedkoop, G. van der Laan, M. Belakhovsky, C. Moduta, A. Marty, and Y. Samson, Science **284**, 2166 (1999).
[22] M. J. Frieser, IEEE Trans. Magn. **4**, 152 (1968).
[23] H. Ebert, Rep. Prog. Phys. **59**, 1665 (1996).
[24] J. P. Hannon, G. T. Trammel, M. Blume, and D. Gibbs, Phys. Rev. Lett. **61**, 1245 (1988); **62**, 2644(E) (1989).
[25] S. W. Lovsey and S. P. Collins, *X-Ray Scattering and Absorption in Magnetic Materials* (Oxford University Press, Oxford, 1996).
[26] L. Néel, J. Phys. Radium **15**, 376 (1954).
[27] C. Liu, E. R. Moog, and S. D. Bader, Phys. Rev. Lett. **60**, 2422 (1988).
[28] D. Weller, J. Stöhr, R. Nakajim, A. Carl, M. G. Samant, C. Chappert, R. Mety, P. Beauillain, P. Veillet, and G. A. Held, Phys. Rev. Lett. **75**, 3752 (1995).
[29] S.-K. Kim, V. A. Chernov, and Y. M. Koo, J. Magn. Magn. Mater. **170**, L7 (1997).
[30] R. Q. Wu and A. J. Freeman, J. Magn. Magn. Mater. **2000**, 498 (1999).
[31] G. Y. Guo, Phys. Rev. B **55**, 11 619 (1997).
[32] R. W. James, *The Optical Principles of the Diffraction of X-Rays* (Ox Bow Press, Woodbridge, CT, 1982), p. 53.
[33] C. Giorgetti, E. Dartyge, C. Brouder, F. Baudelet, C. Meyer, S. Pizzini, A. Fontaine, and R.-M. Galera, Phys. Rev. Lett. **75**, 3186 (1995).
[34] P. Kuiper, B. G. Searle, R. Rudolf, L. H. Tjeng, and C. T. Chen, Phys. Rev. Lett. **70**, 1549 (1993).
[35] A. Scholl, J. Stöhr, J. Luning, J. W. Seo, J. Fompeyrine, H. Siegwart, J.-P. Locquet, G. Nolting, S. Anders, E. E. Fullerton, M. R. Scheinfein, and H. A. Padmore, Science **287**, 1014 (2000).
[36] M. M. Schwickert, G. Y. Guo, M. A. Tomaz, W. L. O'Brien, and G. R. Harp, Phys. Rev. B **58**, R4289 (1998).
[37] See, for example, J. Zak, E. R. Moog, C. Liu, and S. D. Bader, Phys. Rev. B **43**, 6423 (1991); **46**, 5883(E) (1992).
[38] L. Séve, N. Jaouen, J. M. Tonnerre, D. Raoux, F. Bartolomé, M. Arend, W. Felsh, A. Rogalev, J. Goulon, C. Gautier, and J. F. Bérar, Phys. Rev. B **60**, 9662 (1999).
[39] S.-K. Kim and J. B. Kortright (unpublished).
[40] V. Chakarian, Y. U. Idzerda, and C. T. Chen, Phys. Rev. B **57**, 5312 (1998).
[41] R. Nakajima, J. Stöhr, and Y. U. Idzerda, Phys. Rev. B **59**, 6421 (1999).
[42] M. Sacchi, C. F. Hague, L. Pasquali, A. Mirone, J.-M. Mariot, P. Isberg, E. M. Gullikson, and J. H. Underwood, Phys. Rev. Lett. **81**, 1521 (1998).
[43] J. B. Kortright and D. L. Windt, Appl. Opt. **27**, 2841 (1988).
[44] L. Parratt, C. Hempstead, and E. Jossem, Phys. Rev. **105**, 1228 (1957).
[45] S. M. Heald and E. A. Stern, Phys. Rev. B **16**, 5549 (1977).
[46] E. A. Stern and K. Kim, Phys. Rev. B **23**, 3781 (1981).
[47] D. O. Smith, J. Appl. Phys. **36**, 1120 (1965).
[48] Subtle distinctions in taking the KKT of the difference $\delta_+ - \delta_-$ rather than each quantity individually are discussed by D. Y. Smith, Phys. Rev. B **13**, 5303 (1976).
[49] These simulations involved systematic variations in the integration range in transforming experimental MOR to MCD and back again, and also transforming simulated analytic MCD spectra to MOR and back again.
[50] B. L. Henke, E. M. Gullikson, and J. C. Davis, At. Data Nucl. Data Tables **54**, 181 (1993), numerical data (in some cases updated since this publication) can be found at http://www-cxro.lbl.gov/optical_constants/
[51] E. E. Fullerton, J. S. Jiang, M. Grimsditch, H. C. Sowers, and S. D. Bader, Phys. Rev. B **58**, 12 193 (1998).
[52] C. T. Chen, Y. U. Idzerda, H. J. Lin, G. Meigs, A. Chaiken, G. A. Prinz, and G. H. Ho, Phys. Rev. B **48**, 642 (1993).
[53] Y. U. Idzerda, C. T. Chen, S. F. Cheng, W. Varva, G. A. Prinz, G. Meigs, H. J. Lin, and G. H. Ho, J. Appl. Phys. **76**, 6525 (1994).
[54] V. Chakarian, Y. U. Idzerda, G. Meigs, E. E. Chaban, G. A. Prinz, J. H. Park, and C. T. Chen, Phys. Rev. B **53**, 11 313 (1996).
[55] C. S. Nelson, G. Srajer, J. C. Lang, C. T. Venkataraman, S. K. Sinha, H. Hasizume, N. Ishimatsu, and N. Hosoito, Phys. Rev. B **60**, 12 234 (1999).
[56] R. M. Osgood III, S. K. Sinha, J. W. Freeland, Y. U. Idzerda, and S. D. Bader, J. Appl. Phys. **85**, 4619 (1999).
[57] G. H. Vineyard, Phys. Rev. B **26**, 4146 (1982).
[58] S. K. Sinha, E. B. Sirota, S. Garoff, and H. B. Stanley, Phys. Rev. B **38**, 2297 (1988).